Atomistically Modeling the Chemical Potential of Small Molecules in Dense Systems

Gyula Dömötör and Reinhard Hentschke*

Fachbereich Physik und Institut für Materialwissenschaften, Bergische Universität Wuppertal, Gauss-Strausse 20, D-42097 Wuppertal, Germany

Received: September 15, 2003; In Final Form: October 24, 2003

We test a simple grid-search method, in combination with the usual Widom test-particle insertion procedure, to enhance the efficiency of the latter for dense liquids that consist of small molecules. We use simple-point-charge/extended water at different temperatures as an example to illustrate the various aspects that affect the performance. Speed-up factors of up to 100 allow the excess chemical potential to be computed in this very dense system while maintaining the basic simplicity of Widom's method.

1. Introduction

The chemical potential (μ) is one of the most useful quantities about which to have information. There are numerous computer simulation methods for determining the chemical potential of a species in a fluid system that has low or medium density.[1] Possibly the simplest—and, therefore, commonly used—method is the test-particle insertion method that was suggested by Widom[2] and separately by Jackson and Klein.[3] Subsequently, the original derivation in the canonical ensemble was extended to other ensembles (cf. Section 7.2.2 in the work of Frenkel and Smit[4]). In the canonical ensemble, the chemical potential follows from $\mu = \mu_{id} + \mu_{ex}$, where μ_{id} is the ideal gas contribution, and the excess component is given by

$$\beta\mu_{ex} = -\ln\left\langle \frac{1}{V}\int_V \mathrm{d}^3 r_{N+1} \exp[-\beta\Delta u(\vec{r}_{N+1})]\right\rangle_N \qquad (1)$$

Here, $\Delta u(\vec{r}_{N+1})$ is the interaction energy of a virtual particle at position $\vec{r}_{N+1}$, inserted in a configuration produced during a *NVT* simulation, where N is the particle number, V the volume, and T the temperature (from $\beta = (k_B T)^{-1}$), with the remaining N particles in the system. Notice that, here, we assume spherically symmetric interactions. A weakness this method shares with the other methods mentioned previously is the bad convergence of eq 1 as the density becomes high. In fact, it is difficult to find a method that is not impractical for the calculation of the excess chemical potential of pure water and other molecular liquids with comparable or higher density. In such cases, it seems that one must resort to a combination of methods, such as test-particle insertion plus thermodynamic coupling parameter integration.[5] Here, however, we study a much simpler approach, which first identifies, in each configuration, those rare spatial regions, where the integral in eq 1 becomes large. These "holes", where a test particle or molecule may be inserted, are found via a grid search. Subsequently, Monte Carlo (MC) integration is performed over the neighboring lattice cells. For water, which has been used here as an example, we achieve an acceleration that may be up to 2 orders of magnitude in excess to the straightforward Widom method.

We note that Deitrich et al.[6] suggested a conceptually analogous approach for Lennard-Jones liquids. The basic idea in ref 6, as well as that in our work, coincide. Instead of performing straightforward Widom test-particle insertion (or something similar), where the entire configuration integral is performed for the test particle, one first determines where the integration "makes sense". In ref 6, the authors do this by determining, with considerable effort, the excluded volume in the Lennard-Jones fluid, by assigning a hard core radius to every particle. The grid search, which we use, is simpler and faster. Speed is important, as will become clear below. We also perform our calculation for an important molecular system: water. In addition, even though the aforementioned paper claims a speed that is similar to that of this work, the reference contains no evidence to support this claim. In this work, the main effort is expended to do just this, which is a nontrivial problem.

2. Method

We focus on eq 1, which applies to the canonical ensemble; however, the application of the method to other ensembles is completely analogous. First, we note that the MC integration of $\int \mathrm{d}^3 r_{N+1}$ is not essential. Even the selection of a single fixed insertion position $\vec{r}_{N+1}$ anywhere inside the volume V will yield the correct result, provided we average over a sufficiently large number of system configurations (assuming ergodicity). This, however, is wasteful, as long as our method for computing $\int \mathrm{d}^3 r_{N+1}$ is not significantly more expensive than the generation of uncorrelated system configurations.

The basic idea of our method rests on the premise that there are only a few "holes" in every configuration that contribute to the integral; i.e., at these locations, the expression $\exp[-\beta\Delta u]$ exceeds a certain value ϵ. Because we are talking about molecules, or rather about small molecules with little conformational freedom, we must consider their orientation inside V. Thus, a "hole" is characterized by its position as well as its orientation. For every system configuration, we evaluate $\int \mathrm{d}^3 r_{N+1}\, \mathrm{d}\Omega_{N+1}$, which now includes position and orientation (note that $\int \mathrm{d}\Omega = 1/(8\pi^2) \int_0^{2\pi} \mathrm{d}\alpha \int_0^{\pi} \sin\beta \int_0^{2\pi} \mathrm{d}\gamma = 1$, where α, β, and γ are Euler angles) in two steps:

(1) The aforementioned integral is evaluated on N_e nodes of a simple cubic grid with a lattice spacing a, thereby storing those grid coordinates for which

$$\exp[-\beta\Delta u(\vec{r}_{N+1}, \Omega_{N+1})] \geq \epsilon \qquad (2)$$

* Author to whom correspondence should be addressed. E-mail: hentschk@uni-wuppertal.de.

10.1021/jp0367427 CCC: $27.50 © 2004 American Chemical Society
Published on Web 01/22/2004

(in this work: $\epsilon = 0.1$; cf. the discussion given below). Here, the argument Ω_{N+1} refers to one in l possible orientations of the test molecule. In the following, our test molecule is water, and, in this case, $\vec{r}_{N+1}$ refers to the position of the O atom, whereas the $l = 12$ orientations are chosen as follows. The $l = 1$ orientation corresponds to the water molecule lying parallel to the *xy* plane; the bisector of the valence angle is parallel to the $x-$axis. The $l = 2$, 3, and 4 orientations correspond to 90°, 180°, and 270° rotations around an axis through the O atom parallel to the *z*-axis. For $l = 5-12$, this procedure is repeated with the *xy* plane first replaced by the *yz* plane and subsequently by the *xz* plane.

(2) Every node $i = 1, 2, ..., P$ found to fulfill the condition depicted ineq 2, using the *l*-value that yields the lowest Δu value, now is taken to be the center of a cubic cell *i* with volume $v_i = a^3$. The integral $\int_v \mathrm{d}^3 r_{N+1}\, \mathrm{d}\Omega_{n+1}...$ is then calculated via the expression

$$\int_V \mathrm{d}^3 r_{N+1}\, \mathrm{d}\Omega_{N+1} \exp[-\beta \Delta u(\vec{r}_{N+1}, \Omega_{N+1})] \cong \sum_{i=1}^{P} \int_{v_i} \mathrm{d}^3 r_{N+1}\, \mathrm{d}\Omega_{N+1} \exp[-\beta \Delta u(\vec{r}_{N+1}, \Omega_{N+1})] \quad (3)$$

The integrations on the right side of eq 3 are performed via MC integration; i.e.,

$$\int_{v_i} \mathrm{d}^3 r_{N+1}\, \mathrm{d}\Omega_{N+1} \exp[-\beta \Delta u] \cong \frac{v_i}{M} \sum_{j=1}^{M} \exp[-\beta \Delta u(\vec{r}_{N+1;j}, \Omega_{N+1;j})] \quad (4)$$

Here, the index *j* refers to the randomly selected positions and orientations.

The two parameters *a* and *M* both influence the quality and efficiency of the method, whereas the value of ϵ turns out to be of little importance for the quality, as we show in the next section, but it may be chosen to further enhance the efficiency.

3. Simulation Results

The results presented here were obtained using 125 simple-point-charge/extended (SPC/E) water molecules[7] in a periodic cell. Molecular dynamics (MD) simulations were performed using the modeling package AMBER (Assisted Model Building with Energy Refinement, Version 4.1).[8] Temperature and pressure were adjusted via the weak coupling method that is attributed to Berendsen et al.[9] (a temperature relaxation time of 0.2 ps and a pressure relaxation time of 0.2 ps, using the isothermal compressibility of liquid water). This method for temperature and pressure control is numerically very stable; however, it does not produce configurations that correspond to any of the usual ensembles, except for the microcanonical ensemble in the limit of vanishing coupling. Nevertheless, in the present case, this effect should be small (O(1/*N*)), and we use the expression for μ_{ex} that is appropriate in the canonical NPT ensemble to analyze our MD configurations:[10]

$$\beta \mu_{ex} = -\ln\left[\frac{1}{\langle V \rangle} \langle \int_V \mathrm{d}^3 r_{N+1}\, \mathrm{d}\Omega_{N+1} \exp[-\beta \Delta u] \rangle\right] \quad (5)$$

Figure 1 shows μ_{ex} computed according to eq 5, as a function of the average density of MC insertions ρ_{MC} for three selected configurations of our SPC/E water system. The temperature is 300 K, the pressure is 1 bar, and the residue-based cutoff distance for water−water interaction is $r_{cut} = 7$ Å. For every

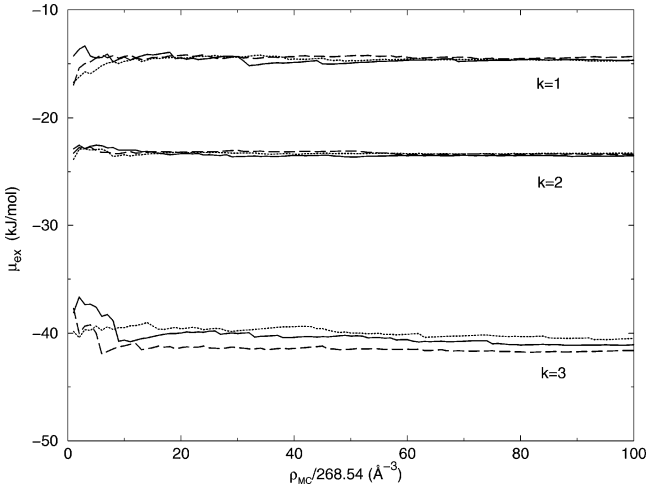

Figure 1. Excess chemical potential (μ_{ex}) computed according to eq 5 versus the average density of Monte Carlo (MC) insertions (ρ_{MC}), for three selected configurations ($k = 1$, 2, 3) extracted from a 100-ps molecular dynamics (MD) simulation of single-point-charge/extended (SPC/E) water at a temperature of 300 K and a pressure of 1 bar ((—) no grid used, (- - -) $a = 0.5$ Å, and (···) $a = 1.0$ Å).

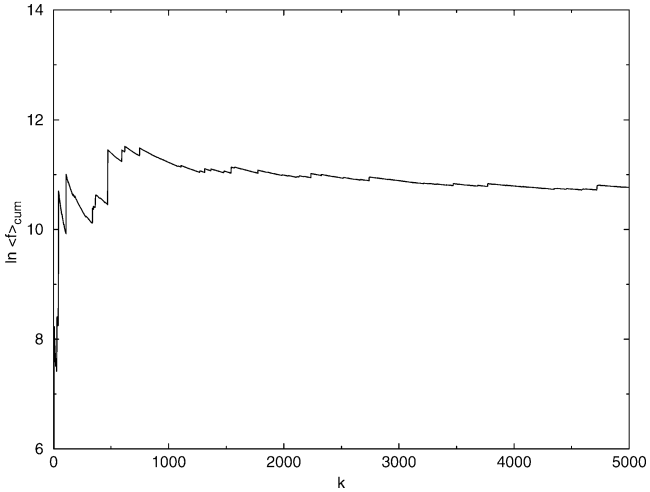

Figure 2. Logarithm of the cumulative average of f ($\ln\langle f\rangle_{cum}$) versus the number of configurations (k) considered in the average.

configuration, one of the curves was obtained by omitting step 1 of the algorithm (i.e., no grid is constructed) and the MC integration, using the given point density ρ_{MC}, extends over the entire volume of the simulation box. This result is compared to two curves that are obtained using grids with different *a* values but with the same ρ_{MC} value within each of the cells *i* in eq 3. The figure illustrates that the μ_{ex} value, obtained in the limit of large ρ_{MC}, are substantially different for the three shown configurations. For a particular configuration, however, the deviations between the curves obtained with and without the grid-search method are small. Here, the lattice constants of 0.5 and 1.0 Å are approximate. What we really do is divide the simulation volume into cells of size a^3, such that $a^{-1}V^{1/3}$ is an integer.

Figure 2 shows the cumulative average of the logarithm of $f \equiv \exp[-\beta\mu_{ex}]$, $\ln\langle f\rangle_{cum}$, as a function of the number of configurations *k*. The system is the same as that in Figure 1, and the time difference between neighboring configurations is 0.1 ps. Here, we use the 0.5-Å grid and a MC point density of $\rho_{MC} \approx 5.4 \times 10^3$ Å^{-3}. We observe that the number of configurations necessary to reach a plateau value for $\langle f\rangle_{cum}$ is quite large. This is because the fluctuations of *f*, expressed via

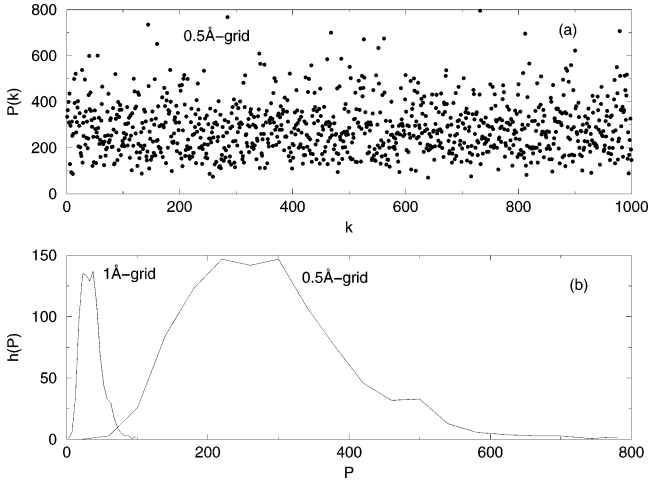

Figure 3. (a) Number of "holes" ($P(k)$) detected on a 0.5-Å grid versus configuration number (k). (b) Number distribution of holes ($h(P)$) versus P for the two indicated grids.

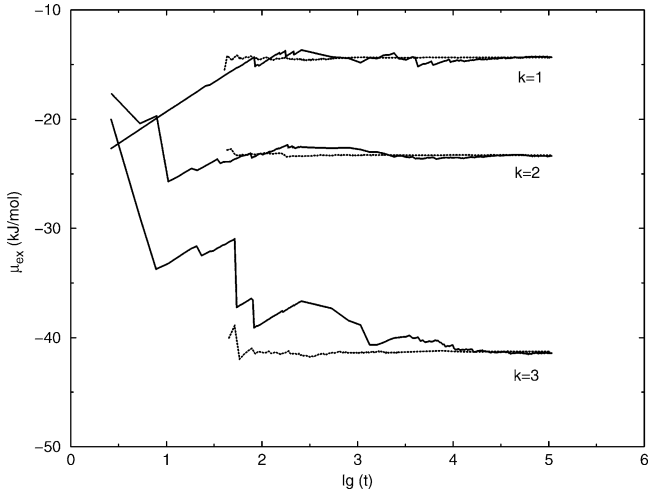

Figure 4. Comparison of (···) our grid method with (—) the straightforward Widom test-particle insertion method for the same three configurations as those in Figure 1. Here, t is the computer processing unit (CPU) time (in seconds).

the relation $\sigma_f = \sqrt{\bar{f}^2 - (\bar{f})^2}$, are large; i.e., the value of μ_{ex} varies strongly between different configurations (cf. Figure 1). This also underscores the fact that a fast evaluation of $\int_V d^3r_{N+1}\, d\Omega_{N+1}...$ is necessary for efficient calculation.

Figure 3a shows the number of holes per configuration k ($P(k)$) for a run at a temperature of $T = 300$ K and pressure of $P = 1$ bar, obtained with a 0.5-Å grid. The configurations were extracted every 20 ps. The corresponding number distribution of holes is shown in Figure 3b, together with the distribution obtained for a 1.0-Å grid. Notice that the distribution for the 0.5-Å grid is rather broad and slightly skewed toward larger $P(k)$ values. However, on average, the observed $P(k)$ values show that the proposed method has the potential to produce a significant acceleration. The distribution for the 1.0-Å grid is narrower and shifted to lower k values on this scale. The shift factor is $\sim 8 = 2^3$, which indicates that both grids do find essentially the same holes (i.e., the relevant holes do seem to have diameters large enough for both grid sizes). This is consistent with the rather good agreement for the two grid sizes in Figure 1.

Figure 4 again shows μ_{ex}, computed according to eq 5, in a direct comparison to the straightforward Widom method. The same three configurations as those in Figure 1 are used. The

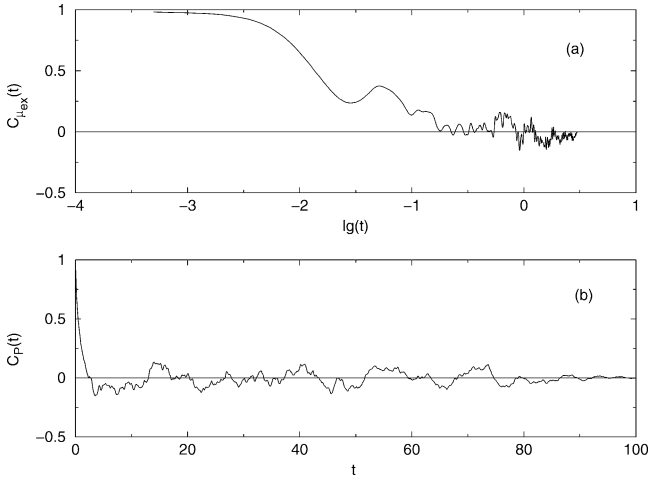

Figure 5. Autocorrelation functions (a) $C_{\mu_{ex}}(t)$ vs t and (b) $C_P(t)$ vs t; the time t in each is given in picoseconds.

value of μ_{ex} for a particular time t means that this value was obtained based on t seconds of computer processing unit (CPU) time. Note that the grid method (here, $a = 0.5$ Å) converges significantly faster than the straightforward Widom method. To quantify this statement, we use the following procedure. Using $\mu_{ex}(t_f)$ obtained for each particular method and configuration at $t_f \approx 10^5$ as a reference value, we determine the time t_0 beyond which $\mu_{ex}(t)$ remains within 5% of the reference value. The ratio of t_0(Widom method) to t_0(grid method) then defines the acceleration for this particular configuration. In total, we have determined the acceleration factors for 10 independent configurations. The resulting average is 67, with a standard error of 29. Notice that, currently, a significant reduction of the standard error—a factor 10 requires the inclusion of 1000 independent configurations—is prohibitively time-consuming.

It is important to note that there are two characteristic times, the ratio of which determines whether the present method is useful or not (compared to the conventional Widom method): t_g, which is the time necessary to generate one statistically independent system configuration, and t_a, which is the time necessary to measure the chemical potential in this configuration with a given precision. The method proposed here solely improves upon t_a. Thus, our method is useful only under the simultaneous conditions: t_a(our method) $\ll$ t_a(conventional method), as we have just shown for the straightforward Widom method, and $t_g \ll t_a$(our method), which we discuss in the next paragraph!

First, we estimate t_g using the autocorrelation function:

$$C_A(k) = \frac{\sum_{i=1}^{K-k} (A_i - \bar{A})\,(A_{i+k} - \bar{A})}{\sum_{i=1}^{K-k} (A_i - \bar{A})^2} \qquad (6)$$

where A_i is given by $\mu_{ex,i}$ and $\bar{A}$ is given by the average over all $\mu_{ex,i}$, including all configurations $i = 1, ..., K$. Notice, however, that this is not the true average value of μ_{ex}, which we use throughout with this exception, because $\langle \ln f \rangle \neq \ln \langle f \rangle$! Figure 5a shows the parameter $C_{\mu_{ex}}(t)$ computed based on the system trajectory again obtained at $T = 300$ K and for $P = 1$ bar. We find that the decrease of $C_{\mu_{ex}}$ vs t is surprisingly rapid. From Figure 5a, we estimate a relaxation time of $\sim$0.1 ps. This is surprising if one thinks of rotational relaxation for water, which is on the order of 10—20 ps at room temperature. Similar

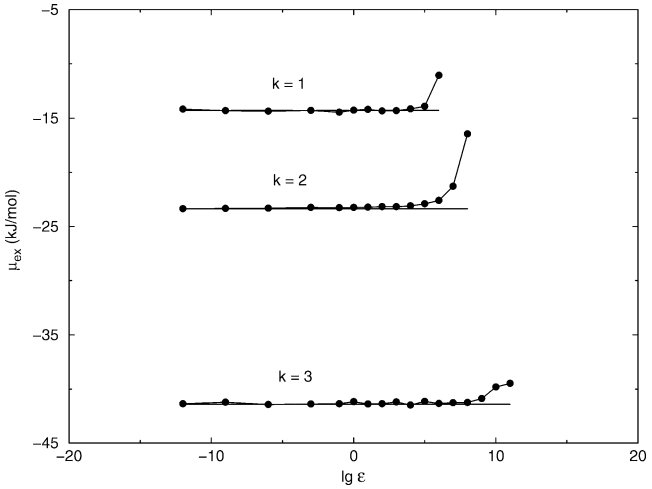

Figure 6. Plot of μ_{ex} vs ϵ for the three configurations shown in Figure 1.

relaxation times are obtained if one computes $C_P(k)$ vs k, where the index P here refers to the number of holes per configuration k (cf. Figure 5b). In this case, A_i represents the number of holes in configuration i and $\bar{A}$ is the corresponding average number of holes. Nevertheless, the necessary shape fluctuations of the holes do not seem to require extensive translation or rotation of the molecules. Thus, using a time step of 10^{-3} ps, ~1 s of CPU time on our work station per statistically independent configuration is required (i.e., $t_g \approx 1$ s). This must be compared with t_a(our method) $\equiv t_0 \approx 70$ s, which is the average t_a value, based on the 10 configurations mentioned previously. This shows that, indeed, both of the aforementioned criteria are met.

Finally, Figure 6 illustrates the dependence of μ_{ex} on the parameter ϵ in eq 2. Again, we use the three configurations used in Figures 1 and 4. Notice that we observe the breakdown of the cutoff criterion defined in eq 2 only for very large values of ϵ. In all three cases, there is a wide plateau spanning many decades, where μ_{ex} is virtually independent of ϵ. The figure emphasizes the dominant contribution of large values of $\exp(-\beta\Delta u)$ to the chemical potential. Thus, increasing the size of ϵ may be used to further enhance the speed of the computation.

Using the grid method, we have computed the excess chemical potential of neat water versus temperature. Figure 7 compares our results (filled circles) for μ_{ex} obtained in SPC/E water to experimental values $\mu_{ex}^{(exp)}$ (solid line). The experimental values were obtained via thermodynamic integration along the following path:

(a) Starting at $T = 273.15$ K and a pressure of 0.0061 bar on the gas−liquid co-existence curve, we approximate the chemical potential at this state point by the ideal gas chemical potential, via the relation $\mu_{id} = \mu_{id}^{(trans)} + \mu_{id}^{(rot)}$. Here, $\mu_{id}^{(trans)} = RT \ln(\beta P \Lambda_T^3)$, where Λ_T is the thermal wavelength, and $\mu_{id}^{(rot)} = -RT \ln q^{(rot)}$, where

$$q^{(rot)} = \frac{(2k_B T)^{3/2}(\pi I_1 I_2 I_3)^{1/2}}{\sigma \hbar^3} \qquad (7)$$

is the classic rotational partition function appropriate for water ($\sigma = 2$). The I_i terms are the principal moments of inertia.

(b) After crossing from the gas to the liquid, using the entropy and enthalpy of vaporization given in ref 11, we continue along the gas−liquid co-existence curve via integration of the heat capacity c_P, which is tabulated in the same reference, to obtain the enthalpy. Similarly, we obtain the entropy via integration of the c_P/T relationship.

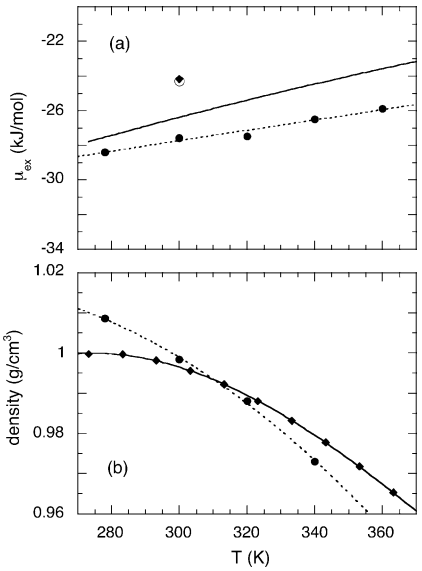

Figure 7. (a) Plot of μ_{ex} vs T for neat water, in comparison to SPC/E water at a pressure of 1 bar ((●) simulation results based on 3×10^5 configurations each, (- - -) linear least-squares approximation, and (—) experimental $\mu_{ex}^{(exp)}$ value obtained as described in the text. Additional *NVT*-simulation results are also indicated ((○) from Hermans et al.[14] and (♦) from Baez and Clancy[15]). (b) Temperature dependence of the density ((●) simulation results and (♦) experimental values). Lines in both panels represent simple polynomial approximations.

TABLE 1: Experimental Chemical Potential ($\mu^{(exp)}$) and the Corresponding Excess Chemical Potential ($\mu_{ex}^{(exp)}$) in Neat Water (at a Pressure of 1 bar), Computed According to the Procedure Explained in the Text

temperature, T (K)	$\mu^{(exp)}$ (kJ mol^{-1})	$\mu_{ex}^{(exp)}$ (kJ mol^{-1})
273.15	−53.44	−27.80
283.15	−54.10	−27.26
293.15	−54.78	−26.74
303.15	−55.48	−26.23
313.15	−56.22	−25.73
323.15	−56.97	−25.25
333.15	−57.75	−24.78
343.15	−58.55	−24.32
353.15	−59.38	−23.88
363.15	−60.22	−23.45
373.15	−61.09	−23.02

(c) At $T = 373.15$ K and a pressure of 1 bar, which is the pressure used in our simulation, we use the c_P values that have been tabulated versus temperature (at a pressure of 1 bar) in ref 12 to obtain the chemical potential values $\mu^{(exp)}$ compiled in Table 1. The excess chemical potential is obtained using the relation $\mu_{ex}^{(exp)}(T) = \mu(T)^{(exp)} - \mu_{id}^{(trans)}(T) - \mu_{id}^{(rot)}(T)$ (cf. Table 1).

In Figure 7, the so-computed $\mu_{ex}^{(exp)}$ is shown as a solid line. Note that our values for $\mu_{ex}^{(exp)}$ agree with the values given in ref 13 (this reference provides values only in the range of 273.15−318.15 K). We find that the SPC/E values for μ_{ex} fall below the experimental values. The differences range from ~$0.5RT$ at low temperatures to ~$0.7RT$ at high temperatures. The error in the simulation results is probably best-represented by the deviations of the points from the straight-line fit (dashed line in Figure 7). Also included in Figure 7a are two simulation results for μ_{ex} obtained using the SPC/E model in a *NVT* simulation: the hollow circle represents data from ref 14, and the solid diamond represents data from ref 15. For the sake of

completeness, and as an accuracy check, we have included the density as a function of temperature in Figure 7b. The experimental values were taken from ref 12.

4. Conclusion

We have tested a simple grid-search method to enhance the efficiency of the ordinary Widom test-particle insertion approach. The method turns out to increase efficiency by as much as a factor of 100 for liquid water. Even though there are three parameters that must be adjusted to the system of interest, the simplicity of the method makes it very appealing, when the excess chemical potential in a dense liquid of small molecules must be computed repeatedly.

Acknowledgment. This work was supported through BMBF Grant No. 03D0073C (Langzeitbeständige Hochleistungsverbundsysteme). One of the authors (GD) thanks the financial support of OTKA T 032190.

References and Notes

(1) King, P. M. In *Computer-Simulation of Biomolecular Systems. Theoretical and Experimental Applications*; van Gunsteren, W. F., Weiner, P. K., Wilkinson, A. J., Eds.; ESCOM Science Publishers B.V.: Leiden, The Netherlands, 1993; Vol. 2.

(2) Widom, B. *J. Chem. Phys.* **1963**, *39*, 2802.

(3) Jackson, J. L.; Klein, L. S. *Phys. Fluids* **1984**, *7*, 228.

(4) Frenkel, D.; Smit, B. *Understanding Molecular Simulation*; Academic Press: New York, 1986.

(5) Knopp, B.; Suter, U. W.; Gusev, A. A. *Macromolecules* **1997**, *30*, 6107.

(6) Deitrich, G. L.; Scriven, L. E.; Davis, H. T. *J. Chem. Phys.* **1989**, *90*, 2370.

(7) Berendsen, H. J. C.; Grigera, J. R.; Straatsma, T. P. *J. Chem. Phys.* **1987**, *91*, 6269.

(8) Pearlman, D. A.; Case, D. A.; Caldwell, J. W.; Ross, W. S.; Cheatham, T. E., III; Ferguson, D. M.; Seibel, G. L.; Singh, U. C.; Weiner, P. K.; Kollman, P. A. AMBER4.1. University of California, San Francisco, CA, 1995.

(9) Berendsen, H. J. C.; Postma, J. P.; van Gunsteren, W. F.; DiNola, A.; Haak, J. R. *J. Chem. Phys.* **1984**, *81*, 3684.

(10) Shing, K. S.; Chung, S. T. *J. Chem. Phys.* **1987**, *91*, 1674.

(11) D'Ans·Lax *Taschenbuch für Chemiker und Physiker, Band I—Physikalisch—Chemische Daten*; Lechner, M. D., Ed.; Springer: Berlin, 1992.

(12) Lide, D. R.; Kehiaian, H. V. *CRC Handbook of Thermophysical and Thermochemical Data*; CRC Press: Boca Raton, FL, 1994.

(13) Ben-Naim, A.; Marcus, Y. *J. Chem. Phys.* **1984**, *81*, 2016.

(14) Hermans, J.; Pathiaseril, A.; Anderson, A. *J. Am. Chem. Soc.* **1988**, *110*, 5982.

(15) Baez, L. A.; Clancy, P. *J. Chem. Phys.* **1995**, *103*, 9744.